THE JOURNAL OF PHYSICAL CHEMISTRY A

Article

pubs.acs.org/JPCA

Ground-State Charge Transfer: Lithium−Benzene and the Role of Hartree−Fock Exchange

Carlos H. Borca,[†] Lyudmila V. Slipchenko,*[,†] and Adam Wasserman*[,†,‡]

[†]Department of Chemistry, Purdue University, 560 Oval Drive, West Lafayette, Indiana 47907, United States

[‡]Department of Physics and Astronomy, Purdue University, 525 Northwestern Avenue, West Lafayette, Indiana 47907, United States

Supporting Information

ABSTRACT: Most approximations to the exchange-correlation functional of Kohn−Sham density functional theory lead to delocalization errors that undermine the description of charge-transfer phenomena. We explore how various approximate functionals and charge-distribution schemes describe ground-state atomic-charge distributions in the lithium−benzene complex, a model system of relevance to carbon-based supercapacitors. To understand the trends, we compare Hartree−Fock (HF) and correlated post-HF calculations, confirming that the HOMO−LUMO gap is narrower in semilocal functionals but widened by hybrid functionals with large fractions of HF exchange. For semilocal functionals, natural bond orbital (NBO) and Mulliken schemes yield opposite pictures of how charge transfer occurs. In PBE, for example, when lithium and benzene are <1.5 Å apart, NBO yields a positive charge on the lithium atom, but the Mulliken scheme yields a negative charge. Furthermore, the partial charges in conjugated materials depend on the interplay between the charge-distribution scheme employed and the underlying exchange-correlation functional, being critically sensitive to the admixture of HF exchange. We analyze and explain why this happens, discuss implications, and conclude that hybrid functionals with an admixture of about one-fourth of HF exchange are particularly useful in describing charge transfer in the lithium−benzene model.

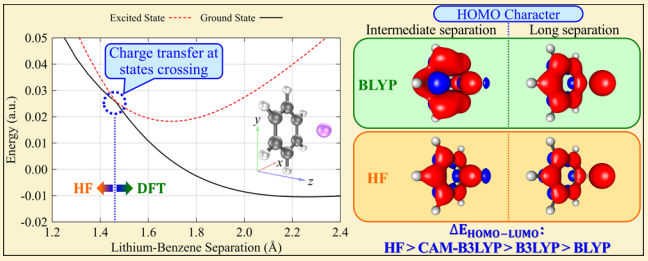

1. INTRODUCTION

Porous carbon materials have great potential for the construction of novel electric energy storage (EES) devices such as supercapacitors.[1−3] Because of experimental limitations, high costs of nanotechnology research, and importance of quantum effects, computational-aided fabrication of carbon materials for supercapacitors is promising.[4−7] Often, classical force fields provide useful data for calculations of chemical stability, adsorption and desorption dynamics, and other properties of these materials.[8] Yet the exploration of quantum phenomena such as charge transfer, which is at the heart of the working mechanism of supercapacitors, requires ab initio treatment. The goal of this study is to investigate whether standard approximations in Kohn−Sham density functional theory (KS-DFT),[9,10] when used in combination with popular charge-distribution schemes,[11] provide an adequate description of the ground-state charge transfer that occurs in a very simple model system: the lithium−benzene complex. Some of the key features observed in this system are due to the interaction between a lithium atom that can be easily ionized and a benzene ring whose valence electrons are delocalized due to aromaticity, so our observations are relevant to the much more complex simulations of carbon nanoporous electrodes in supercapacitors,[12] where such interactions are ubiquitous. More generally, we want to determine how different charge-distribution schemes perform for various families of approximate exchange-correlation (XC) functionals and understand the trends.

KS-DFT is an extraordinarily popular electronic structure method applied throughout science and engineering.[13] As is well known, however, approximate KS-DFT calculations suffer from problems that need to be addressed.[14] For instance, most standard approximations to the XC functional underestimate charge-transfer excitation energies and overestimate binding energies of charge-transfer complexes.[15,16] Mori-Sánchez et al.[17] and Cohen et al.[18] demonstrated that this problem can be traced back to the delocalization error of approximate functionals: their tendency to minimize the energy by unrealistically spreading-out the electronic density, especially at large separations between the fragments involved in the charge transfer. As discussed by Cohen et al.,[15] this inaccuracy is closely related to the self-interaction error, and it is caused by the unphysical convex behavior of the energy as a function of fractional charge.

Properties of alkali-conjugated complexes have been explored in several computational studies.[19−25] For instance, studying the conformation of complexes of lithium and C60 fullerenes, Varganov et al. found a strong ionic interaction between the atom and the fullerene.[26] The structures and dissociation

Received: September 6, 2016
Revised: September 22, 2016
Published: September 23, 2016

DOI: 10.1021/acs.jpca.6b09014
J. Phys. Chem. A 2016, 120, 8190−8198

energies of lithium and benzene sandwich complexes were researched by Vollmer et al. using several quantum-mechanical methods.[20] Kang studied the formation of neutral lithium-aromatic complexes and found that it originates in the charge transfer from the lithium atom to the aromatic rings.[21] An emerging discussion about the existence of charge transfer between lithium and aromatic carbon compounds motivated Ferre-Vilaplana[22] and Martinez et al.[23] to look into the lithium−benzene complex. Marshall et al. explored cation-π interactions, modeling the approach of alkali cations to a benzene ring from different angles and inclinations, pointing out that nonperpendicular interactions in cation−benzene complexes are attractive.[24]

In response to the controversy about charge transfer, Baker and Head-Gordon[27] studied a set of polyaromatic carbon systems with lithium, which included the lithium−benzene complex, and suggested that some density-functional approximations may produce artificial charge transfer due to the self-interaction error, whereas Hartree−Fock (HF) underestimates the amount of charge transfer as a result of overlocalization. Inspired by that work, Denis and Iribarne[28] used the lithium−benzene complex as a prototype system to understand the interaction in lithium-doped carbon compounds, focusing on the relationship between its symmetry and stability. Employing highly sophisticated techniques, they concluded that charge transfer does indeed occur.

We ask two questions that are relevant in this context: (1) What do popular charge-distribution schemes such as NBO, MPA, and ChElPG tell us about ground-state charge transfer in the lithium−benzene complex? (2) How does the answer to question (1) depend on the approximation employed for the XC functional? As will be made clear, the admixture of HF exchange in the functional plays a critical role. Resorting to HF and post-HF multistate calculations, we explain why. First, we summarize in the next section the computational methods employed.

2. COMPUTATIONAL METHODS

Ground-state electron transfer is studied as a function of the separation between a lithium atom and the center of a benzene ring. A potential energy rigid scan (PES) is performed along the coordinate of separation between the center of mass (COM) of the benzene molecule and the lithium atom, perpendicular to the plane of benzene (see Figure 1). This is done in a series of unrestricted single-point calculations,[29] where the lithium atom advances toward the benzene molecule along the main symmetry axis, while the geometry of the benzene molecule, optimized with B3LYP/6-31G*, is kept fixed. The atom starts its path toward the ring at 7.0 Å, moving at 0.1 Å steps, and totaling 71 points. Initial separation of 7.0 Å guarantees minimal interaction between the two fragments. The electronic structure and the atomic charge on lithium are analyzed as a function of separation. For consistency, all calculations are carried out with the same basis set, 6-31G*, in the computational chemistry package Q-Chem 4.3.[30−32] The self-consistent field convergence criteria are chosen such that the Direct Inversion in the Iterative Subspace error is below 1.0×10^{-9}. For each geometry, the lowest energy solution was found by employing the maximum overlap method (MOM)[33] when necessary.

Two sets of approximate functionals are employed. Each set has functionals from different rungs in Perdew's Jacob's ladder of approximations[13] or levels of sophistication. On the one hand, PES calculations are performed with PBE,[34] PBE0,[35] PBE50,[36] and LRC-ωPBEPBE[37] functionals. PBE is a non-empirical generalized gradient approximation (GGA) with exchange and correlation expressions derived from physical constraints. The hybrids PBE0 and PBE50 are prepared by admixing 25 and 50% of E_x^{HF}, respectively, as this inclusion is believed to improve atomization energies, energy barriers, and energy gaps in materials without impacting computational performance.[38,39] A different way of including a fraction of E_x^{HF} in hybrids is through the long-range correction (LRC), as in LRC-ωPBEPBE. In LRC functionals, the $1/r_{12}$ dependence of the exchange potential is decomposed into an error function of ωr_{12}, which accounts for the amount of E_x^{HF} and governs the long-range behavior, and its complementary, which corresponds to pure-DFT-exchange, E_x^{DFT}, and rules short-range interactions. ω is a range-separation parameter that adjusts the distance at which the E_x^{DFT} vanishes.

On the other hand, BLYP,[40] B3LYP,[41] and CAM-B3LYP[42] were used. BLYP is a simple GGA constructed by putting together the pure-DFT Becke88-exchange[43] and the Lee−Yang−Parr correlation[44] functionals. Replacing the exchange with a mixture of Slater-,[9,10,45] Becke88-, and HF-exchange and combining VWN5-[46] and LYP-correlation produces the highly popular B3LYP hybrid. CAM-B3LYP is another LRC hybrid prepared by using the Coulomb Attenuated Method (CAM) for long-range exchange correction. The decomposition of $1/r_{12}$ in the calculation of E_x is done by including two parameters. The second parameter avoids vanishing of E_x^{HF} at short distances and of E_x^{DFT} at long distances. Notably, CAM-B3LYP does not include Slater-exchange, as opposed to B3LYP.

In addition to the KS-DFT calculations, lithium−benzene interaction energies are computed with HF, second- and fourth-order Møller−Plesset perturbation theory (MP2, MP4),[47] and coupled-cluster with single and double excitations method (CCSD).[48,49]

To better understand charge-transfer behavior, we employ the equation-of-motion coupled-cluster method with single and double excitations for electron attachment (EOM-EA-CCSD).[50−52] EOM-EA-CCSD provides information on both ground- and excited-state PESs, allowing us to relate charge-transfer to the interaction of the ground state and the excited states that have charge-transfer character. Chemically important

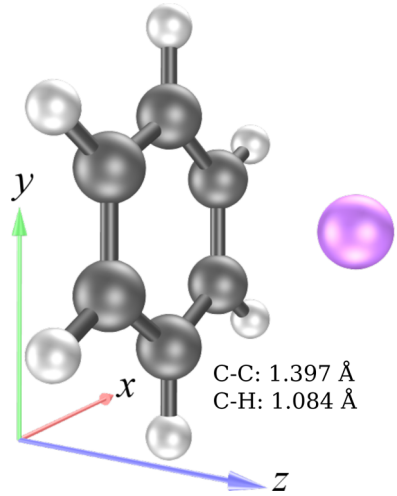

Figure 1. Lithium−benzene complex. The lithium atom is displaced along the z axis toward the center of the benzene ring.

DOI: 10.1021/acs.jpca.6b09014
J. Phys. Chem. A 2016, 120, 8190−8198

regions of the excited-state PESs are computed on a tighter grid, such that the whole PES comprises 221 points computed with uneven displacements ranging from 0.005 to 0.1 Å.

The partial charge on the lithium atom is computed by means of Mulliken Population Analysis (MPA),[53] natural bonding orbital theory (NBO),[54] Chemical Electrostatic Potentials using a Grid (ChElPG),[55] as well as a simple estimate based on the magnitude of the dipole moment, μ

$$Q_A^{\mu/z}(z) = \frac{\mu}{z} \tag{1}$$

where z is the separation between fragments and $\vec{\mu}$ is the dipole-moment vector defined as

$$\vec{\mu} = \int \mathrm{d}\vec{r}\; n(\vec{r}) z \hat{k} \tag{2}$$

where $n(\vec{r})$ is the ground-state electron density and $\hat{k}$ is the z-direction unitary vector.

Interaction energy curves are calculated as the difference between the total ground-state energy of the system, at each point, and the sum of the energies of the isolated fragments: the benzene molecule and the lithium atom

$$E_{\mathrm{int}}(z) = E_{\bigcirc\cdots\mathrm{Li}}(z) - (E_{\bigcirc} + E_{\mathrm{Li}}) \tag{3}$$

3. RESULTS AND DISCUSSION

We divide the discussion into five parts. The first two parts analyze in detail atomic charges and molecular orbitals (MOs). The next two sections compare (single-state) KS-DFT results with those of a multistate approach. The final section discusses the description interaction energies.

3.1. Charge Distributions. We summarize our results of the charge-distribution analyses in Figure 2, where the reader can verify that the calculated charge on the lithium atom strongly depends on both the nature of the approximate XC functional and the charge-distribution scheme employed. We discuss the latter dependence first.

Interestingly, in Figure 2, natural charges from NBO (blue solid lines) and Mulliken charges (green long-dashed lines) show opposite results. The Mulliken charge on lithium tends to be negative. This can be understood by examining the definition of the Mulliken charge for open-shell systems. The charge belonging to atom A, Q_A^{MPA}, is expressed by

$$Q_A^{\mathrm{MPA}} = Z_A - \sum_{\nu\in A}\sum_{\mu}\sum_{i}(C_{\mu i}^{\alpha} C_{\nu i}^{\alpha *} + C_{\mu i}^{\beta} C_{\nu i}^{\beta *}) S_{\mu\nu} \tag{4}$$

where Z_A is the atomic number of atom A, $C_{\mu i}^{\alpha}$ and $C_{\nu i}^{\alpha *}$ are the matrix elements representing the alpha coefficients of the basis functions μ and ν, respectively, in the ith MO, and $S_{\mu\nu}$ is the matrix element representing the overlap-integral between basis functions μ and ν. The same notation applies for beta orbitals, substituting the α superscript by β. The second term on the right-hand side, often called the gross atomic product, is computed by taking the sums of the product of the coefficients of two basis functions and their overlap. If several basis functions overlap on the lithium atom, which is the case at short distances, the corresponding gross atomic product increases, making the Mulliken charge more negative.

These effects had been previously observed, in general, by Reed et al.[56] and Kim et al.,[57] and, in particular, for the lithium–benzene complex by Vollmer et al.[20] They pointed out that Mulliken populations and charges are highly susceptible to the basis set employed and become ambiguous when utilized with diffuse basis sets.

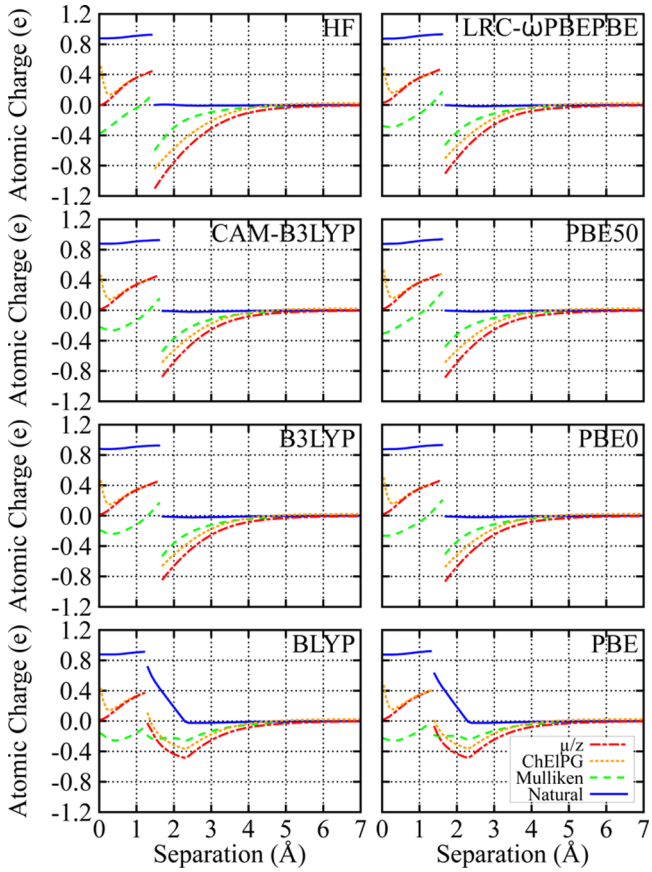

Figure 2. Charge accumulated over the lithium atom as a function of the separation between fragments in the lithium–benzene complex. Noteworthy, charge-distribution schemes produce diverse results. By admixing HF exchange, the description of the charge transfer changes.

ChElPG is an alternative to explore atomic charges. It uses the electrostatic potential (ESP) computed from the system's wave function on a grid and then tries to match that ESP by optimizing a set of trial point charges located at the nuclei. ChElPG curves (orange short-discontinuous lines in Figure 2) are smooth at long and medium distances, in agreement with those of Mulliken. However, as the atom moves toward the cavity formed by the benzene ring, ChElPG shows a sheer behavior when the atom is too close to the ring's surface and the ESP is poorly described.

The dipole-based scheme of eq 1 (red dotted line in Figure 2) agrees qualitatively with Mulliken and ChElPG at medium and large distances, but the scheme clearly breaks down at short separations, where the classical expression for the dipole as generated by point charges is not adequate.

In contrast with other schemes, the variations of the natural charge on the lithium atom are solely due to changes in the occupation of bonding and nonbonding orbitals. In the NBO theory, orbitals are classified into three groups: nonbonding natural atomic orbitals, orbitals involved in bonding and antibonding, and Rydberg-type orbitals. Atomic and Rydberg orbitals are made of basis functions of single atoms, whereas bonding and antibonding orbitals are a combination of basis functions of two atoms. This resembles Lewis' idea of core, lone pair, and valence electrons. Thus, the NBO procedure treats the bonding and antibonding orbitals as linear combinations of

DOI: 10.1021/acs.jpca.6b09014
J. Phys. Chem. A 2016, 120, 8190–8198

two-atom basis functions, while Mulliken analysis treats all of the orbitals as linear combinations of two-atom basis functions.[11] At the end, an orthonormal set of localized maximum-occupancy orbitals is produced. The leading N members of this set give a Lewis-like description of the total electron density.

Notably, the NBO scheme reveals extreme behaviors, showing either no charge accumulation on lithium at long separations or a sudden change in the lithium charge at short separations. BLYP and PBE are the exceptions, showing an intermediate region in which there is an incremental accumulation of positive charge. In all cases, the lithium natural charges at short separations become positive and close to 1 e.

Different charge-distribution schemes thus provide qualitatively different results. Natural charges have the advantage of not being as susceptible to basis-set issues as Mulliken charges or to surface effects as ChElPG charges.[20] As it will be shown in the next section, natural charges are in agreement with the analysis of the MOs for this system.

Figure 2 also provides a comparison between approximate XC functionals of similar complexity. At long distances, all KS-DFT calculations and HF go to the correct separation limit with no partial charges on either fragment. At short separations, all functionals and HF predict charge transfer from lithium to benzene. However, pure-DFT functionals, BLYP and PBE, show a different picture at intermediate separations. Namely, all charge schemes reveal a growth of fractional, positive charge on the lithium atom in the region between 2.3 and 1.3 Å for these two functionals. To understand this, we analyze valence MOs next.

3.2. Frontier Molecular Orbitals. We plot in Figure 3 the energies of relevant alpha MOs. A correlation between the qualitative description of charge transfer described in the previous section, the energy difference between the highest occupied molecular orbital (HOMO) and the lowest unoccupied molecular orbital (LUMO), the character of the frontier MOs, and the contribution of E_x^{HF} becomes evident. For more clarity, we discuss first the results of the functionals of the PBE family, shown on the right-hand side of Figure 3, and compare them with HF (top left).

The HOMO−LUMO gap width at *large* separation follows the trend

$$\text{HF} > \text{LRC}-\omega\text{PBEPBE} > \text{PBE50} > \text{PBE0} > \text{PBE}$$

In general, the gap width decreases due to the stabilization of unoccupied orbitals (dotted lines) and destabilization of occupied orbitals (continuous line) following the same trend. Notably, for separations between 1.3 and 2.3 Å, PBE and BLYP have no gap, promoting delocalization.

As shown in Figure 2, all charge distribution schemes except for NBO show some degree of charge transfer even at medium distances, reflecting HOMO delocalization between the lithium atom and the benzene ring. This is a manifestation of HOMO hybridization. When the character of the HOMO changes, it produces discontinuities in atomic-charge curves. PBE is the most interesting case, so we discuss it in detail using Figure 4, which compares HOMOs, at three characteristic separations, in HF (Figure 4a−c), PBE0 (Figure 4d−f), and PBE (Figure 4g−i). The reader may also refer to the Supporting Information for additional details supporting this discussion.

On the one hand, as shown in the top row of Figure 4, the contribution from benzene's π bonding orbital (or A_{2u}) (here and later benzene orbital symmetries are based on D_{6h} point group) to the long-range HF HOMO increases as the separation shortens, implying that the weight from benzene's basis functions is becoming predominant in the complex. As the atom approaches the ring, larger portions of lithium's p_z and benzene's p_z basis functions are incorporated into the HOMO, at the expense of a smaller share of lithium's s atomic orbitals (compare Figure 4b and c and see Supporting Information). Notwithstanding, we find no evidence of charge transfer in Figure 4b and c because the lithium atom always contributes to the HOMO.

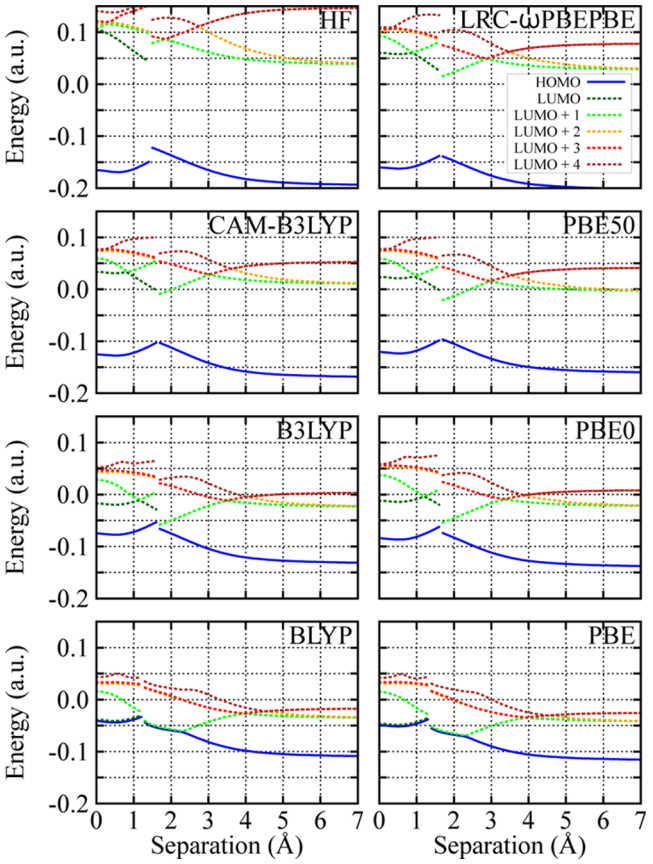

Figure 3. Frontier molecular orbital energies, as a function of the separation between fragments, for each density functional approximation applied to the lithium−benzene complex. When the HF character of the exchange functional increases, the occupied molecular orbitals are stabilized, while the unoccupied orbitals are destabilized.

On the other hand, inspection of the PBE HOMO at the bottom in Figure 4 suggests that at *large* separation it has a main contribution from lithium's s orbital and a minor contribution from benzene's A_{2u} orbital, similar to HF (compare Figure 4c and i and see Supporting Information). Nonetheless, the contribution from p_z orbitals from both lithium and benzene is marginally greater in PBE, while the weight of lithium's s basis functions slightly decreases. This is reflected in a smoother and slightly more spread-out surface of the PBE HOMO over the benzene ring.

At *medium* separations, the character of the HOMO in PBE changes, in contrast with HF (compare Figure 4b and h). Instead of having an important contribution from benzene's π (A_{2u}), we see a predominant π^* (E_{2u}) antibonding character in PBE. In the same range of separations (1.3 to 2.3 Å), HOMO and LUMO energy curves in PBE become degenerate and experience a kink (see Figure 3). In this region, the frontier

DOI: 10.1021/acs.jpca.6b09014
J. Phys. Chem. A 2016, 120, 8190−8198

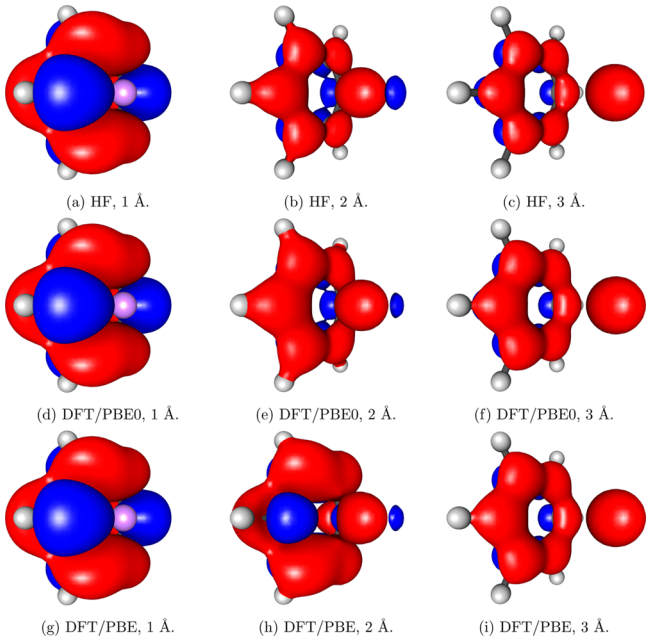

Figure 4. Evolution of the lithium−benzene highest occupied molecular orbital (HOMO) as a function of the separation between fragments, for HF, PBE0, and PBE. The HOMO adopts one character at long separation and another one at short separation in HF and PBE0, whereas in PBE it exhibits three different characters. Interestingly, at separations shorter than 1.3 Å, the HOMO is exclusively localized over the benzene molecule in all cases.

MOs consist of the E_{2u} orbital of benzene and an s-p_z hybridized orbital on lithium (see Figure 4h). Also, natural charges suggest that this intermediate state involves a partial charge transfer between the lithium atom and benzene molecule (see Figure 2).

At *short* separations, PBE predicts complete electron transfer from lithium to benzene. The HOMO localizes over the benzene ring and misses any contribution from lithium's basis functions. Additionally, the character of the HOMO and LUMO changes again (compare Figure 4g and h), and the HOMO−LUMO degeneracy is broken (see Figure 3). Thus, at short separations, PBE and HF show the same charge-transfer state (see Figure 2 and Supporting Information).

The PBE0 HOMO, shown at the center in Figure 4, transforms as the HF HOMO. The main difference of PBE0 with respect to *pure* PBE is the absence of the intermediate-separation state (compare Figure 4e and h). In PBE0, the system abruptly switches from the long-range neutral state to the short-range charge-transfer state at ∼1.65 Å (see Figures 2 and 3). Likewise, the evolution of the HOMO in PBE50 and LRC-ωPBEPBE is analogous to that observed in HF.

The other set of functionals, including BLYP, B3LYP, and CAM-B3LYP, follows the previous description closely, as seen in Figures 2 and 3. As with PBE, an intermediate state is also observed with BLYP. In the BLYP-family functionals, the trend of the HOMO−LUMO gap is

$$\text{HF} > \text{CAM−B3LYP} > \text{B3LYP} > \text{BLYP}$$

Therefore, in both PBE and BLYP families of functionals, the character of the frontier MOs and their energies depend strongly upon the admixture of E_x^{HF}. The difference between the functionals in each set is the proportion of E_x^{HF}. Our calculations show that the HOMO−LUMO gap increases with the amount of E_x^{HF} and is the largest in HF. Additionally, functionals with a narrow HOMO−LUMO gap exhibit an intermediate partial-charge-transfer state. The charge transfer occurs at longer intermonomer separation in functionals with no E_x^{HF}. Is the charge transfer between lithium and benzene a real phenomenon? Which functional and which partial-charge scheme provide the best description of the lithium−benzene complex? We explore these questions in detail in the next two sections of the paper.

3.3. State-Crossing. In the first two sections of this discussion, the variation of charge accumulation on lithium was related to a change in character of the wave function along the lithium−benzene separation. The abrupt change in the wave function character suggests the existence of a state crossing. While the description of a state crossing by single-reference methods is generally nontrivial, a few techniques are available, including wave function stability analysis,[58] symmetry-enforced self-consistent field convergence, constrained DFT methods,[59,60] and so on. To find the lowest energy solution for each separation between lithium and benzene, we employed the MOM by Gilbert et al.[33]

If the MOM is triggered on the first cycle of the self-consistent procedure, it holds the initial configuration by choosing occupancies that maximize the overlap of the new occupied orbitals with the set previously occupied. In our case, when the calculation of the PES starts from long separations, the MOM, accompanied by reading orbitals from a previous geometry, helps maintaining the neutral-state character [⬡···Li·]. On the contrary, starting from short separations, the charge-transfer state [⬡⁻Li⁺] can be enforced and kept.

Electronic energies of the neutral and charge-transfer states obtained with the MOM are presented in Figure 5. The curves are plotted using only those calculations in which the self-consistent field procedure converged under tight criteria. State crossings are clearly observed in all cases except BLYP and PBE, both of which become unstable in the region near the crossing. This instability is manifested by the presence of an intermediate state seen in Figure 3. We note that the convergence of the higher energy state is more stable when the proportion of E_x^{HF} is greater, such that the most stable MOM calculations are those of HF.

Comparison of HF and DFT state-crossing curves suggests that the charge-transfer state in HF is displaced to higher energies with respect to the neutral state, causing a shift of the crossing to shorter separations. Indeed, the crossing occurs at ∼1.65 Å in all hybrid and LRC functionals, whereas in HF it is located at ∼1.45 Å. A relative overstabilization of the charge-transfer state in functionals, with respect to HF, is consistent with narrower HOMO−LUMO gaps in functionals than in HF, as discussed in Section 3.2.

The separation at which the state crossing appears in B3LYP coincides with that at which HOMO and LUMO energies nearly collide in Figure 3. A similar situation is observed for PBE0, although the HOMO−LUMO gap is slightly wider. This suggests that one could correctly *estimate* the position of a state-crossing in PBE0 and B3LYP by monitoring the HOMO−LUMO gap. However, this is not true in general.

3.4. Excited-State Calculations. The calculations discussed hitherto are based on single-referenced methods. To better understand the physics of charge transfer in our model system, we now calculate the interaction of the ground and excited charge-transfer states using a method that is capable of describing several electronic states on equal footing. For this

DOI: 10.1021/acs.jpca.6b09014
J. Phys. Chem. A 2016, 120, 8190−8198

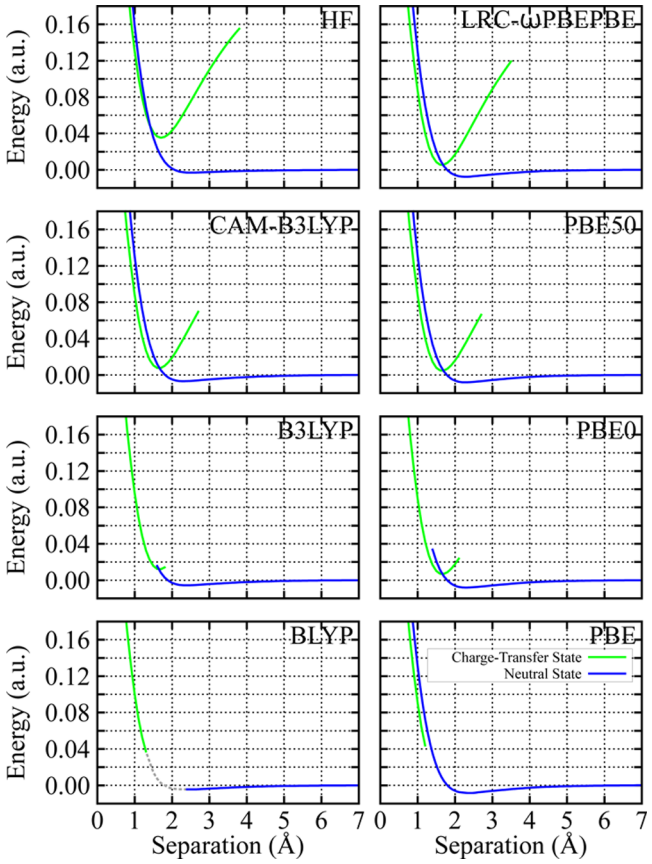

Figure 5. Energy of the electronic states as a function of the separation between the plane of benzene and the lithium atom, obtained by the maximum overlap method. The neutral state is plotted with a blue line. The charge-transfer state is depicted in green.

purpose, it is possible to use a multireference method such as multiconfigurational self-consistent field (MCSCF), multireference perturbation theory (CASPT2, MRPT, MCQDPT), or multireference configuration interaction (MRCI).[61] We use an alternative method for describing electronic states in the lithium−benzene complex, namely, EOM-EA-CCSD. This sophisticated treatment provides a robust description of radical systems, correctly capturing the multiconfigurational nature of electronic states by using a single-reference formalism.[52]

The closed-shell cation state [⬡···Li^+] is taken as a reference state in EOM-EA-CCSD, while electronic states of a neutral complex are obtained by creating an electron on any vacant orbital. These electronic configurations constitute single excitations. Additionally, electronic configurations in which the creation of an electron on a virtual orbital is accompanied by the excitation of another electron (double excitations) are also included in the subspace in which the Hamiltonian is diagonalized. Thus, in the EOM-EA-CCSD formalism both the ground and charge-transfer states of the lithium−benzene complex are obtained as single excitations from the cation reference state and are expected to be described with similar quality. Therefore, EOM-EA-CCSD provides an accurate location of the state crossing if there is one.

The results obtained with the EOM-EA-CCSD method are presented in Figure 6. The character of the electronic states might be derived from the shapes of the singly occupied molecular orbitals (SOMOs) of the leading configuration for each state. For example, in the large-separation limit, one can clearly see electronic states corresponding to excitations on lithium: the $1s^2 2s^1$ ground state (in black), the degenerate pair of $1s^2 2p_x^1$ and $1s^2 2p_y^1$ (in red), and the $1s^2 2p_z^1$ (in orange). A crossing of the ground and charge-transfer states is observed at 1.465 Å. At separations shorter than this, the character of the ground state switches from a neutral state, with the SOMO represented mainly by the 2s orbital of the lithium atom, to a degenerate pair of the charge-transfer states, with the SOMO being one of the π^* orbitals of benzene. Note that the crossing of the ground and charge-transfer states is a real crossing, rather than an avoided crossing because the states involved do not mix by symmetry. This is also true for other state crossings seen in Figure 6. The position of the state crossing between the ground and charge-transfer states predicted by EOM-EA-CCSD better agrees with HF than standard-hybrid or LRC functionals, and it disagrees with the description of pure functionals BLYP and PBE, which exhibit an unphysical intermediate state. In contrast with Mulliken and ChElPG, NBO charges respond consistently with the appearance of the crossing of the neutral and ionic states for each of the hybrid functionals and HF.

However, as it is obvious from Figure 6, the position of the state crossing depends upon the shape and depth of the potential curves of both the ground and charge-transfer states. In particular, overstabilization of the ionic state results in an early charge transfer, as is observed in BLYP and PBE. These functionals produce an intermediate spurious state in which fractional atomic charges increase from 0 to almost 1 in the region between 1.3 and 2.3 Å, as seen in Figure 2. This raises a red flag when using standard KS-DFT for modeling charge transfer in conjugated materials: The functional needs to be carefully selected to predict the charge transfer at the correct separation between moieties, or alternative computational schemes must be used. In the model system considered, B3LYP and PBE0 are close to the correct behavior.

3.5. Interaction Energy. We now turn our attention to the calculation of interaction energies from Equation 3. Figure 7 summarizes our results obtained via correlated wave function methods and various density-functional approximations. As expected, the HF equilibrium distance, ∼2.5 Å, is longer than the distance obtained with CCSD, ∼2.25 Å, both in agreement with those reported by Baker and Head-Gordon.[27] An old experimental study by Manceron and Andrews[62] estimates a separation of ∼1.8 Å based on gas-phase infrared spectra of lithium−benzene in argon, but it is unclear if this corresponds to the neutral or cationic species. A previous in silico study by Vollmer et al.[20] on the neutral complex reports 2.252 Å (black, dashed, vertical line on Figure 7), calculated with MP2(FC)/6-31G(d). Zhengyu et al.[19] reported 2.600 Å with MP2/6-31G and 2.511 Å with HF/6-31G(d).

In agreement with the results by Vollmer et al., we observe that HF underbinds the lithium−benzene complex, highlighting the importance of correlation effects. Our HF interaction energy, −0.0031 a.u., is close to the one they reported at the minimum: −0.0029 a.u.[20] To our knowledge, the most accurate interaction energy in lithium−benzene is −0.0078 a.u. (black, dashed, horizontal line on Figure 7), reported by Denis and Iribarne,[28] who calculated it at the CCSD(T)/CBS level, including corrections for core correlation and relativistic effects. Vollmer et al.[20] reported a value of −0.0092 a.u. using the G3(MP2)[63] method.

We now compare against our CCSD interaction curve to meaningfully contrast the results from different methods without the influence of basis set and basis-set superposition

DOI: 10.1021/acs.jpca.6b09014
J. Phys. Chem. A 2016, 120, 8190−8198

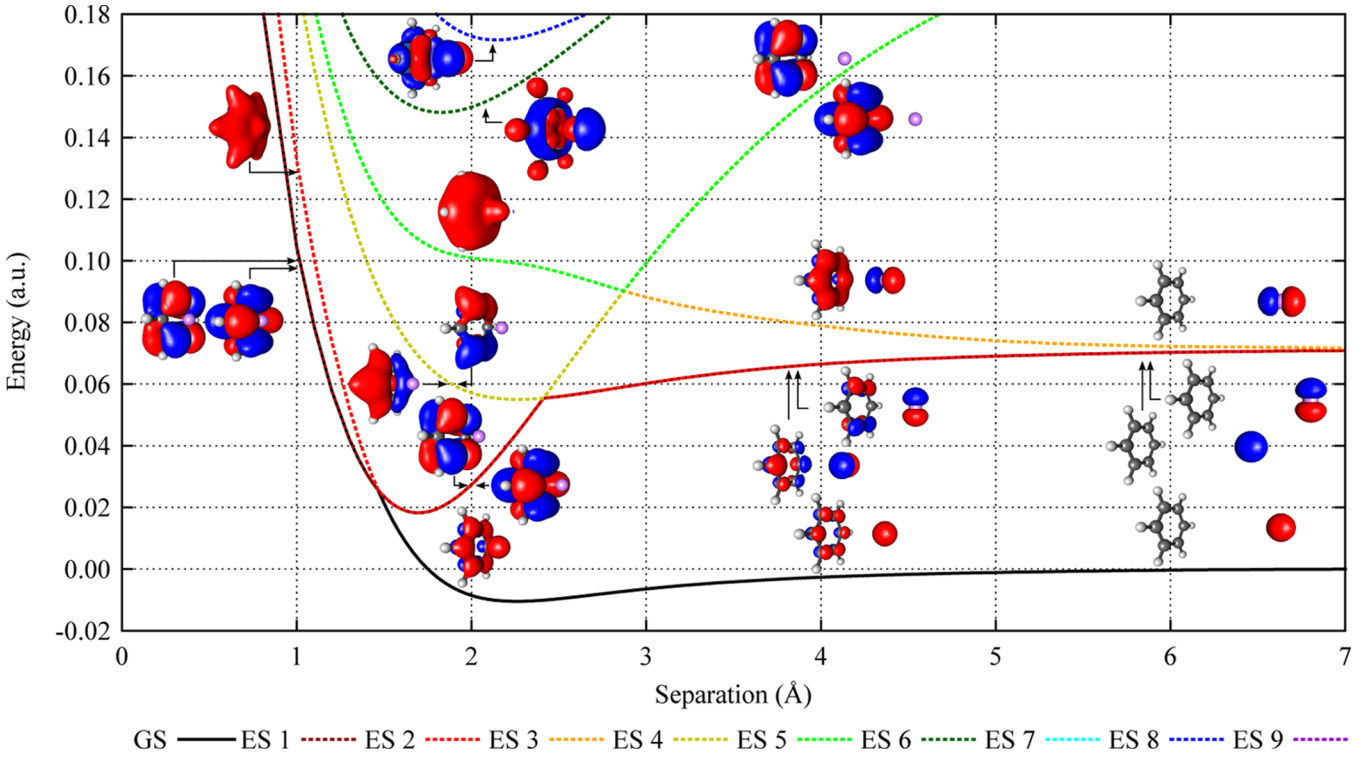

Figure 6. Energy of the electronic states as a function of the separation between the plane of benzene and the lithium atom, obtained by the EOM-EA-CCSD method. The ground-state (GS) is plotted with a continuous black line. Dotted lines represent the first nine excited states (ESs). Singly occupied molecular orbitals (SOMOs) corresponding to the leading configuration of each state are shown at several separations. A crossing between the long-separation ground state, in which the SOMO is mainly localized over lithium, and a charge-transfer state, in which the SOMO localizes exclusively over the benzene molecule, occurs at about 1.5 Å.

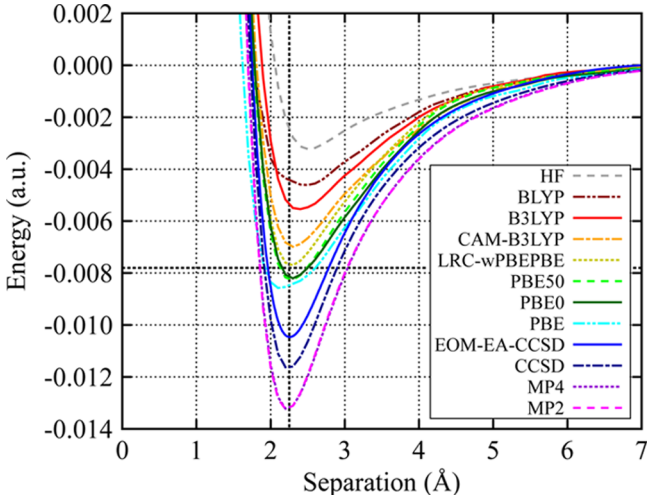

Figure 7. Interaction energy of the lithium−benzene complex computed by different methods. The black dotted horizontal line corresponds to the most accurate interaction energy in lithium−benzene found in the literature.[28] The black dotted vertical line indicates the most accurate equilibrium distance.[27] All results of the present work are obtained in 6-31G* basis.

errors. The minimum energy from our CCSD calculation is −0.0114 a.u. and the separation at that point is 2.2 Å. MP2 and MP4 show very similar results and their curves overlap in Figure 7. Also, MP2 calculations agree with those of Vollmer et al.[20] Nonetheless, it is known that the MP methods may overestimate the dispersion energy[8] and overbind the complex.

In general, approximate DFT calculations do better than HF, but they still underbind the complex when compared to CCSD. Even though GGAs and standard hybrids account for local and semilocal correlation, the long-range part of correlation is not properly described.[11] Functionals derived from PBE show similar interaction-energy curves, with a slight decrease in the binding energy when the amount of E_x^{HF} increases. That is, the binding energy follows the trend

$$\text{HF} < \text{LRC}-\omega\text{PBEPBE} < \text{PBE50} \approx \text{PBE0} < \text{PBE}$$

The PBE binding energy shows an unphysical wide well near the equilibrium separation. This is because the character of the PBE ground state changes near the equilibrium distance (compare Figure 4b and h), such that the repulsive side of the well is determined by the intermediate state with partial charge-transfer character. In other functionals of the PBE family and in HF, this intermediate state does not exist and the charge transfer occurs at a shorter-than-equilibrium distance, such that neither the interaction energy nor the equilibrium position is affected by the charge-transfer phenomenon.

A rather unexpected behavior is observed in BLYP-related functionals. The CAM-corrected functional describes the interaction energy better than either B3LYP or BLYP. Thus the trend is opposite to that of PBE-related functionals: The binding energy in the BLYP-derived functionals increases with the proportion of E_x^{HF}. It is hard to point out the exact origin of the difference because neither E_x nor E_c is easily comparable between BLYP-related functionals. Finally, similar to PBE, the BLYP binding curve exhibits a wider well due to a state crossing near the equilibrium separation.

DOI: 10.1021/acs.jpca.6b09014
J. Phys. Chem. A 2016, 120, 8190−8198

4. CONCLUSIONS

We assessed how several functionals model ground-state charge transfer and predict charge distributions in the lithium−benzene complex. This model illustrates an all-too-common problem in computational chemistry: With results hinging on a delicate combination of methods, the interplay of approximate functionals and charge-distribution schemes can lead to drastically different qualitative pictures of ground-state charge transfer.

Functionals with an admixture of E_x^{HF} are useful in describing charge transfer in the lithium−benzene complex. The HOMO−LUMO gap is widened when the proportion of E_x^{HF} is increased, a consequence of the stabilization of the occupied MOs and the destabilization of the unoccupied MOs.

Despite the existence of a state crossing that induces charge transfer, the crossing occurs in the repulsive region of the interaction curve, leaving the equilibrium region unaffected in hybrid functionals and HF. However, the equilibrium region is incorrectly described by pure functionals PBE and BLYP because of a crossing with an artificial state. Ground-state charge distributions display sharp features when state crossings occur, as is clear from Figures 2 and 5.

While modeling the state crossing is prone to errors when using single-reference methods, high computational cost might hinder the use of multireference or excited-state methods for larger systems relevant in materials science. In those situations, rigorous functionals capable of describing charge-transfer phenomena, or alternative computational schemes, are needed.

■ ASSOCIATED CONTENT

Supporting Information

The Supporting Information is available free of charge on the ACS Publications website at DOI: 10.1021/acs.jpca.6b09014.

Plots of the contributions from s and p_z atomic orbitals on lithium to the HOMO of lithium−benzene as a function of the separation between fragments. (PDF)

■ AUTHOR INFORMATION

Corresponding Authors

*L.V.S.: E-mail: lslipchenko@purdue.edu.

*A.W.: E-mail: awasser@purdue.edu.

Notes

The authors declare no competing financial interest.

■ ACKNOWLEDGMENTS

We thank Martín A. Mosquera and Benjamin T. Nebgen. A.W. acknowledges support from the Office of Basic Energy Sciences, U.S. Department of Energy, under grant no. DEFG02-10ER16196. L.V.S. acknowledges support of the National Science Foundation, grant no. CHE-1465154 and Purdue University. This research was supported in part through computational resources provided by Information Technology at Purdue University.

■ REFERENCES

(1) Conway, B. E. *Electrochemical Supercapacitors: Scientific Fundamentals and Technological Applications (POD)*; Kluwer Academic/Plenum: New York, 1999; pp 193−195.

(2) An, K. H.; Kim, W. S.; Park, Y. S.; Moon, J.-M.; Bae, D. J.; Lim, S. C.; Lee, Y. S.; Lee, Y. H. Electrochemical Properties of High-power Supercapacitors Using Single-walled Carbon Nanotube Electrodes. *Adv. Funct. Mater.* **2001**, *11*, 387−392.

(3) Goodenough, J. B.; Abruña, H. D.; Buchanan, M. V. *Basic Research Needs for Electrical Energy Storage: Report of the Basic Energy Sciences Workshop for Electric Energy Storage*; U.S. Department of Energy, Office of Basic Energy Science, 2007.

(4) Kalugin, O. N.; Chaban, V. V.; Loskutov, V. V.; Prezhdo, O. V. Uniform Diffusion of Acetonitrile Inside Carbon Nanotubes Favors Supercapacitor Performance. *Nano Lett.* **2008**, *8*, 2126−2130.

(5) Shim, Y.; Kim, H. J. Nanoporous Carbon Supercapacitors in an Ionic Liquid: A Computer Simulation Study. *ACS Nano* **2010**, *4*, 2345−2355.

(6) Shim, Y.; Jung, Y. J.; Kim, H. J. Graphene-based Supercapacitors: A Computer Simulation Study. *J. Phys. Chem. C* **2011**, *115*, 23574−23583.

(7) Feng, G.; Cummings, P. T. Supercapacitor Capacitance Exhibits Oscillatory Behavior as a Function of Nanopore Size. *J. Phys. Chem. Lett.* **2011**, *2*, 2859−2864.

(8) Lewars, E. *Computational Chemistry*; Springer, 2010.

(9) Hohenberg, P.; Kohn, W. Inhomogeneous Electron Gas. *Phys. Rev.* **1964**, *136*, B864.

(10) Kohn, W.; Sham, L. J. Self-consistent Equations Including Exchange and Correlation Effects. *Phys. Rev.* **1965**, *140*, A1133.

(11) Jensen, F. *Introduction to Computational Chemistry*; Wiley, 2007.

(12) Thackeray, M. M.; Wolverton, C.; Isaacs, E. D. Electrical Energy Storage for Transportation - Approaching the Limits of, and Going Beyond, Lithium-ion Batteries. *Energy Environ. Sci.* **2012**, *5*, 7854−7863.

(13) Perdew, J. P. Climbing the Ladder of Density Functional Approximations. *MRS Bull.* **2013**, *38*, 743−750.

(14) Burke, K. Perspective on Density Functional Theory. *J. Chem. Phys.* **2012**, *136*, 150901.

(15) Cohen, A. J.; Mori-Sánchez, P.; Yang, W. Insights into Current Limitations of Density Functional Theory. *Science* **2008**, *321*, 792−794.

(16) Roy, L. E.; Jakubikova, E.; Guthrie, M. G.; Batista, E. R. Calculation of One-electron Redox Potentials Revisited. Is It Possible to Calculate Accurate Potentials with Density Functional Methods? *J. Phys. Chem. A* **2009**, *113*, 6745−6750.

(17) Mori-Sánchez, P.; Cohen, A. J.; Yang, W. Localization and Delocalization Errors in Density Functional Theory and Implications for Band-gap Prediction. *Phys. Rev. Lett.* **2008**, *100*, 146401.

(18) Cohen, A. J.; Mori-Sánchez, P.; Yang, W. Fractional Charge Perspective on the Band Gap in Density-functional Theory. *Phys. Rev. B: Condens. Matter Mater. Phys.* **2008**, *77*, 115123.

(19) Zhengyu, Z.; Jian, X.; Chuansong, Z.; Xingming, Z.; Dongmei, D.; Kezhong, Z. Theoretical Study of Inner-sphere Reorganization Energy of the Electron Transfer Reactions Between M-C6H6 and M^+-C6H6 Complexes in the Gas Phase: An *Ab Initio* Computation. *J. Mol. Struct.: THEOCHEM* **1999**, *469*, 1−6.

(20) Vollmer, J. M.; Kandalam, A. K.; Curtiss, L. A. Lithium-benzene Sandwich Compounds: A Quantum Chemical Study. *J. Phys. Chem. A* **2002**, *106*, 9533−9537.

(21) Kang, H. S. Density Functional Study of Lithium-aromatic Sandwich Compounds and Their Crystals. *J. Phys. Chem. A* **2005**, *109*, 478−483.

(22) Ferre-Vilaplana, A. Storage of Hydrogen Adsorbed on Alkali Metal Doped Single-layer All-carbon Materials. *J. Phys. Chem. C* **2008**, *112*, 3998−4004.

(23) Martinez, J. I.; Cabria, I.; López, M. J.; Alonso, J. A. Adsorption of Lithium on Finite Graphitic Clusters. *J. Phys. Chem. C* **2009**, *113*, 939−941.

(24) Marshall, M. S.; Steele, R. P.; Thanthiriwatte, K. S.; Sherrill, C. D. Potential Energy Curves for Cation-π Interactions: Off-Axis Configurations Are Also Attractive. *J. Phys. Chem. A* **2009**, *113*, 13628−13632.

(25) Olivares-Amaya, R.; Stopa, M.; Andrade, X.; Watson, M. A.; Aspuru-Guzik, A. Anion Stabilization in Electrostatic Environments. *J. Phys. Chem. Lett.* **2011**, *2*, 682−688.

(26) Varganov, S. A.; Avramov, P. V.; Ovchinnikov, S. G. Ab Initio Calculations of Endo-and Exohedral C60 Fullerene Complexes with Li

DOI: 10.1021/acs.jpca.6b09014
J. Phys. Chem. A 2016, 120, 8190−8198

+ Ion and the Endohedral C60 Fullerene Complex with Li2 Dimer. *Phys. Solid State* **2000**, *42*, 388−392.
(27) Baker, T. A.; Head-Gordon, M. Modeling the Charge Transfer Between Alkali Metals and Polycyclic Aromatic Hydrocarbons Using Electronic Structure Methods. *J. Phys. Chem. A* **2010**, *114*, 10326−10333.
(28) Denis, P. A.; Iribarne, F. C2v or C6v: Which Is the Most Stable Structure of the Benzene-lithium Complex? *Chem. Phys. Lett.* **2013**, *573*, 15−18.
(29) Foresman, J. B.; Frisch, A. E. *Exploring Chemistry with Electronic Structure Methods*; Gaussian, Inc.: Pittsburgh, PA, 1996; pp 171−172.
(30) Shao, Y.; Molnar, L. F.; Jung, Y.; Kussmann, J.; Ochsenfeld, C.; Brown, S. T.; Gilbert, A. T.; Slipchenko, L. V.; Levchenko, S. V.; O'Neill, D. P.; et al. Advances in Methods and Algorithms in a Modern Quantum Chemistry Program Package. *Phys. Chem. Chem. Phys.* **2006**, *8*, 3172−3191.
(31) Shao, Y.; Gan, Z.; Epifanovsky, E.; Gilbert, A. T.; Wormit, M.; Kussmann, J.; Lange, A. W.; Behn, A.; Deng, J.; Feng, X.; et al. Advances in Molecular Quantum Chemistry Contained in the Q-chem 4 Program Package. *Mol. Phys.* **2015**, *113*, 184−215.
(32) Krylov, A. I.; Gill, P. M. W. Q-Chem: An Engine for Innovation. *Wiley Interdiscip. Rev.: Comput. Mol. Sci.* **2013**, *3*, 317−326.
(33) Gilbert, A. T. B.; Besley, N. A.; Gill, P. M. W. Self-Consistent Field Calculations of Excited States Using the Maximum Overlap Method (MOM). *J. Phys. Chem. A* **2008**, *112*, 13164−13171.
(34) Perdew, J. P.; Burke, K.; Ernzerhof, M. Generalized Gradient Approximation Made Simple. *Phys. Rev. Lett.* **1996**, *77*, 3865−3868.
(35) Adamo, C.; Scuseria, G. E.; Barone, V. Accurate Excitation Energies from Time-dependent Density Functional Theory: Assessing the PBE0Model. *J. Chem. Phys.* **1999**, *111*, 2889−2899.
(36) Bernard, Y. A.; Shao, Y.; Krylov, A. I. General Formulation of Spin-flip Time-dependent Density Functional Theory Using Non-collinear Kernels: Theory, Implementation, and Benchmarks. *J. Chem. Phys.* **2012**, *136*, 204103.
(37) Henderson, T. M.; Janesko, B. G.; Scuseria, G. E. Generalized Gradient Approximation Model Exchange Holes for Range-separated Hybrids. *J. Chem. Phys.* **2008**, *128*, 194105.
(38) Perdew, J. P.; Ernzerhof, M.; Burke, K. Rationale for Mixing Exact Exchange with Density Functional Approximations. *J. Chem. Phys.* **1996**, *105*, 9982−9985.
(39) Liu, F.; Proynov, E.; Yu, J.-G.; Furlani, T. R.; Kong, J. Comparison of the Performance of Exact-exchange-based Density Functional Methods. *J. Chem. Phys.* **2012**, *137*, 114104.
(40) Miehlich, B.; Savin, A.; Stoll, H.; Preuss, H. Results Obtained with the Correlation Energy Density Functionals of Becke and Lee, Yang and Parr. *Chem. Phys. Lett.* **1989**, *157*, 200−206.
(41) Becke, A. D. Density-functional Thermochemistry. III. The Role of Exact Exchange. *J. Chem. Phys.* **1993**, *98*, 5648−5652.
(42) Yanai, T.; Tew, D. P.; Handy, N. C. A New Hybrid Exchange-correlation Functional Using the Coulomb-attenuating Method (CAM-B3LYP). *Chem. Phys. Lett.* **2004**, *393*, 51−57.
(43) Becke, A. D. Density-functional Exchange-energy Approximation with Correct Asymptotic Behavior. *Phys. Rev. A: At., Mol., Opt. Phys.* **1988**, *38*, 3098.
(44) Lee, C.; Yang, W.; Parr, R. G. Development of the Colle-Salvetti Correlation-energy Formula into a Functional of the Electron Density. *Phys. Rev. B: Condens. Matter Mater. Phys.* **1988**, *37*, 785.
(45) Slater, J. C. *The Self-Consistent Field for Molecules and Solids*; McGraw-Hill: New York, 1974; *Vol. 4*.
(46) Vosko, S. H.; Wilk, L.; Nusair, M. Accurate Spin-dependent Electron Liquid Correlation Energies for Local Spin Density Calculations: A Critical Analysis. *Can. J. Phys.* **1980**, *58*, 1200−1211.
(47) Møller, C.; Plesset, M. S. Note on an Approximation Treatment for Many-electron Systems. *Phys. Rev.* **1934**, *46*, 618.
(48) Pople, J. A.; Krishnan, R.; Schlegel, H. B.; Binkley, J. S. Electron Correlation Theories and Their Application to the Study of Simple Reaction Potential Surfaces. *Int. J. Quantum Chem.* **1978**, *14*, 545−560.
(49) Bartlett, R. J.; Purvis, G. D. Many-body Perturbation Theory, Coupled-pair Many-electron Theory, and the Importance of Quadruple Excitations for the Correlation Problem. *Int. J. Quantum Chem.* **1978**, *14*, 561−581.
(50) Stanton, J. F.; Bartlett, R. J. The Equation of Motion Coupled-cluster Method. A Systematic Biorthogonal Approach to Molecular Excitation Energies, Transition Probabilities, and Excited State Properties. *J. Chem. Phys.* **1993**, *98*, 7029−7039.
(51) Nooijen, M.; Bartlett, R. J. Equation of Motion Coupled Cluster Method for Electron Attachment. *J. Chem. Phys.* **1995**, *102*, 3629−3647.
(52) Krylov, A. I. Equation-of-motion Coupled-cluster Methods for Open-shell and Electronically Excited Species: The Hitchhiker's Guide to Fock Space. *Annu. Rev. Phys. Chem.* **2008**, *59*, 433−462.
(53) Mulliken, R. S. Electronic Population Analysis on LCAO [Single Bond] Mo Molecular Wave Functions. I. *J. Chem. Phys.* **1955**, *23*, 1833.
(54) Reed, A. E.; Weinstock, R. B.; Weinhold, F. Natural Population Analysis. *J. Chem. Phys.* **1985**, *83*, 735.
(55) Breneman, C. M.; Wiberg, K. B. Determining Atom-centered Monopoles from Molecular Electrostatic Potentials. The Need for High Sampling Density in Formamide Conformational Analysis. *J. Comput. Chem.* **1990**, *11*, 361−373.
(56) Reed, A. E.; Curtiss, L. A.; Weinhold, F. Intermolecular Interactions from a Natural Bond Orbital, Donor-acceptor Viewpoint. *Chem. Rev.* **1988**, *88*, 899−926.
(57) Kim, D.; Hu, S.; Tarakeshwar, P.; Kim, K. S.; Lisy, J. M. Cation-π Interactions: A Theoretical Investigation of the Interaction of Metallic and Organic Cations with Alkenes, Arenes, and Heteroarenes. *J. Phys. Chem. A* **2003**, *107*, 1228−1238.
(58) Paldus, J.; Čížek, J. Stability Conditions for the Solutions of the Hartree-Fock Equations for Atomic and Molecular Systems. Application to the Pi electron Model of Cyclic Polyenes. *J. Chem. Phys.* **1967**, *47*, 3976−3985.
(59) Wu, Q.; Van Voorhis, T. Constrained Density Functional Theory and Its Application in Long-range Electron Transfer. *J. Chem. Theory Comput.* **2006**, *2*, 765−774.
(60) Van Voorhis, T.; Kowalczyk, T.; Kaduk, B.; Wang, L.-P.; Cheng, C.-L.; Wu, Q. The Diabatic Picture of Electron Transfer, Reaction Barriers, and Molecular Dynamics. *Annu. Rev. Phys. Chem.* **2010**, *61*, 149−170.
(61) Hirao, K. *Recent Advances in Multireference Methods*; World Scientific, 1999; Vol. *4*.
(62) Manceron, L.; Andrews, L. Infrared Spectra and Structures of Lithium-benzene and Lithium-dibenzene Complexes in Solid Argon. *J. Am. Chem. Soc.* **1988**, *110*, 3840−3846.
(63) Curtiss, L. A.; Redfern, P. C.; Raghavachari, K.; Rassolov, V.; Pople, J. A. Gaussian-3 Theory Using Reduced Møller-Plesset Order. *J. Chem. Phys.* **1999**, *110*, 4703−4709.

DOI: 10.1021/acs.jpca.6b09014
J. Phys. Chem. A 2016, 120, 8190−8198